

# Investigation on Cracking Behavior and Development of a Fracture Model of Ti-47Al-2Nb-2Cr Alloy During Hot Deformation

Zhuohan Cao, Yu Sun, Zhipeng Wan, and Lianxi Hu

(Submitted October 30, 2017; in revised form March 28, 2018; published online August 29, 2018)

When alloys are strained to a certain limit under the plastic deformation, ductile fracture occurs. Whether the required deformation can be put into effect before fracture appears has become a serious concern. A combination of compression tests, ductile fracture criteria as well as finite element simulation (FEM) were employed in this study to establish the fracture initiation prediction model of Ti-47Al-2Nb-2Cr alloy. To obtain the critical fracture strain, a technique was proposed to calculate the data for deformed cylindrical samples through isothermal compression tests in the temperature range between 1223 and 1423 K with strain rates ranging from 0.001 to 1 s<sup>-1</sup>. Five commonly used ductile fracture criteria were compared by FE simulation of compressing tests. It was found that the Brozzo criterion was found to be suitable and accordingly a failure criterion, considering temperature and strain ratio was established. Hot working parameters (critical fracture value and critical strain) in deformation could be obtained through the finite element simulation, revealing that this newly established failure criterion could accurately predict cracking initiation in compressing deformation of Ti-47Al-2Nb-2Cr alloy ingot.

**Keywords** fracture model, Ti-47Al-2Nb-2Cr alloy, Zener–Holomon parameter

## 1. Introduction

$\gamma$ -TiAl alloys are considered as a new-generation high-temperature structural materials with application in the aerospace industries as a result of a desired combination of properties like high specific modulus, low density, good creep as well as excellent mechanical properties at elevated temperature (Ref 1-4). Particularly,  $\gamma$ -TiAl alloys present lower density than Ni-based alloy and can work at higher temperature than Ti-based alloy (Ref 5). Thus, they are more likely to supersede conventional superalloy on the aspect of turbine blades and turbocharger disks in advanced powerful engines. However, poor processing ability is the main obstacle for extensive industrial application of  $\gamma$ -TiAl alloy (Ref 6), which is easy to crack even at elevated temperature by conventional hot processing owing to the narrow hot working window (Ref 7) and the structure of intermetallic compounds.

Whether the required deformation on the workpiece can be performed successfully before fracture occurs has become a serious concern in metalworking field. In current industrial processes, a number of undamaged metal products were acquired by trial-and-error method, which is inefficiency, high cost and mostly depends on the engineers' experience (Ref 8-10). Thus, it is quite crucial to investigate the hot mechanical behavior in order to predict and avoid fracture occurrence,

which is one of the main characteristics in the processes of  $\gamma$ -TiAl alloy with poor formability. A series of failure models and criteria have been discussed to predict crack initiation, extension and fracture previously, which mainly consist of three types, namely empirical, cumulative plastic energy and microscale damage models. In empirical models, the fracture models are derived based on the stress and strain. Both Kuhn criterion (Ref 11) and Vujovica–Shabaik criterion (Ref 12) considered that fracture would occur when a strain or stress value came to a critical value. Besides, the cumulative plastic energy models are one of the macroscopic models which introduced a strong coupling between plastic energy collected during deformation and fracture. Freudenthal (Ref 13) suggested that fracture would not occur until cumulative plastic deformation energy arrives to certain critical value. Afterward, Cockcroft (Ref 14) proposed the tensile plastic work criterion along with Latham by compensation of maximum principal stress on the fracture in forming processes. Brozzo et al. (Ref 15) and Oh et al. (Ref 16) modified the Cockcroft–Latham criterion in terms of their experimental results and presented the Brozzo criterion and the Oh criterion covering parameters such as hydrostatic stress and equivalent stress. The microscale damage models are established by McClintock et al. (Ref 17) based on the observation that void initiation and growth followed by coalescence to form a crack. After that, Rice (Ref 18), Oyane (Ref 19) and Ayada et al. (Ref 20) modified different fracture models according to this prototype.

The finite element method (FEM), which can analyze the metal processing efficiently and accurately, has been extensively applied to solve large plastic deformation problems. Thus, the workability of a metal can be analyzed and predicted precisely by an integrated approach consisting of experiments, fracture criteria and FEM technique. Kobayashi and Lee et al. (Ref 21) were one of the precursors who used Cockcroft–Latham criterion and McClintock criterion through FEM technique to analyze the ductile fracture in metal

Zhuohan Cao, Yu Sun, Zhipeng Wan, and Lianxi Hu, National Key Laboratory for Precision Processing of Metals, Harbin Institute of Technology, Harbin 150001, People's Republic of China. Contact e-mails: 1120910311@hit.edu.cn, yusun@hit.edu.cn, 920027930@qq.com, and hulx@hit.edu.cn.

deformation. After that, various applications of computer-based numerical techniques have been studied by many researchers to analyze plastic fracture according to different deformation processes. Wifi et al. (Ref 22, 23) and Fu et al. (Ref 24) studied the accuracy of different fracture criteria in predicting metal-work's fracture problems by combining experiments with FE model.

A failure model considering parameters such as deformation temperature and strain rate is developed in this work to predict the fracture initiation of TiAl alloy, which adopts a combination of theoretical failure criteria and FEM technique.

## 2. Materials and Experimental Procedure

The as-received alloy was made from powder metallurgy technology. The nominal chemical composition is Ti-47Al-2Nb-2Cr (molar fraction, %). According to the analysis of the x-ray diffraction (XRD) pattern as well as the back-scattered electron (BSE) image of starting material as shown in Fig. 1, it illustrates that the alloys consist of  $\gamma$ -TiAl phase (black base) and  $\alpha_2$ -Ti<sub>3</sub>Al phase (white ribbon). The cylindrical specimens intended to be used are 6 mm in diameter and 9 mm in height, which were processed by linear cutting machine. The hot compression experiments were performed on the Gleeble-1500D thermomechanical simulator with temperature of 1223, 1273, 1323, 1373, 1423 K and strain rates of 0.001, 0.01, 0.1, 1 s<sup>-1</sup>. For the aim of eliminating the influence of friction in the deformation processes, graphite lubricant was used on the pressure indenter and two head faces of samples. The actual temperature of sample was controlled by employing a thermocouple spot to weld on the center of the cylindrical sample surface. Obviously, the whole samples heated at a speed of 283 K/s to desired upsetting temperature, were held for 5 min to obtain the uniform and homogenized temperature. During the experiment, as a function of strain, strain rate and temperature, flow stress values could be received continuously by an automatic data acquisition system in a personal computer. After experiments, the deformed samples were immediately water quenched to room temperature so as to preserve the initial deformed microstructure. Each specimen was visually distinguished to make sure the critical fracture reduction on the free surface. What deserved to be mentioned is that classical dichotomy theory was employed in the work to find out the threshold values of fracture strain.

To observe the microstructural evolution and fracture surface, the samples were sectioned vertical to the compression

axis of samples after tests. Microstructure analysis was performed on a Quanta 200FEG electron scanning microscope (SEM) and a JEOL scanning tunnel microscope (STM) after tested samples were grinded, polished and corroded.

By operating the finite element software DEFORM-3D, information like stress-strain history and diverse damage values could be obtained in FEM simulations at each compressing process. In simulations, the useful thermophysical property database of materials was measured and set up, where flow stress information was monitored following hot compression experiments to guarantee the accuracy.

## 3. Results and Discussion

### 3.1 Stress-Strain Behavior

The true stress-strain curves corresponding to 1223-1423 K and 0.001-1.0 s<sup>-1</sup> obtained from thermocompression experiments are revealed in Fig. 2. It demonstrates that peak stress increases observably with the growing strain rate and decreasing temperature. Before reaching the peak stress, the influence of work hardening was obvious because of the increased density of dislocations. With deformation going on, dynamic recovery occurred, where low angle boundaries and sub-grains developed, but the sub-boundaries maintained almost equiaxed. With the continuous deformation, the strain reached a critical point, moreover, dynamically recrystallized grains presented at the original grain boundaries (Ref 25). A driving force for DRX was provided by plastic deformation heat and dislocations, which activated a growing number of potential nuclei, formed new recrystallized grains and refined original microstructure (Ref 26). When dynamic equilibrium between work hardening and softening was acquired, dislocation density maintained invariable and the flow stress became steady.

Generally, the true stress-strain curves mainly present DRX characteristics with obvious peak stresses, which is a matter of balance between working hardening and dynamic softening. Such characterization of flow stress curves can also be widely observed in  $\gamma$ -TiAl alloy (Ref 7) and other alloys such as aluminum alloys (Ref 27, 28). Compared with the flow stress curves in Fig. 2 under different conditions, the flow stress grows with increasing strain rate and decreasing metalworking temperature. An obvious stress decrease after the peaks could be observed due to DRX softening in Fig. 2. A big difference between the flow stress at high strain rate (1 s<sup>-1</sup>) and other low strain rates could be observed. This phenomenon could be

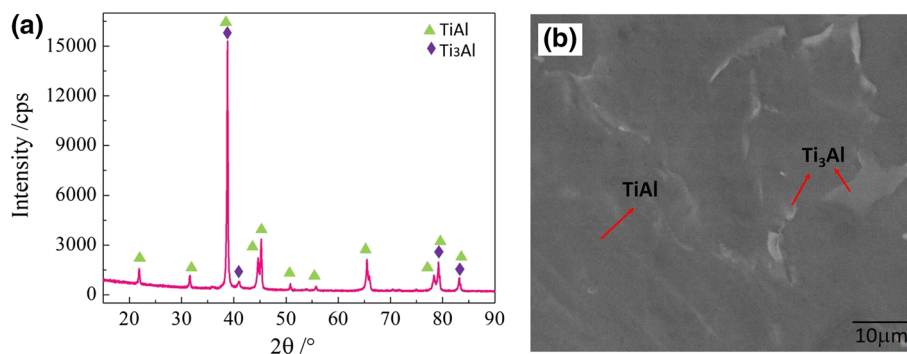


Fig. 1 The XRD pattern (a) and initial microstructure (b) of Ti-47Al-2Nb-2Cr alloy

concerned with the dependence of the DRX type on the deformation parameters.

To calculate the apparent activation energy of deformation, Arrhenius equation for different temperature and strain rates was selected (Ref 13).

$$\dot{\epsilon} = A[\sinh(\alpha\sigma)]^n \exp\left(-\frac{Q}{RT}\right) \quad (\text{Eq 1})$$

where  $\dot{\epsilon}$  is the strain rate ( $\text{s}^{-1}$ ),  $\sigma$  is the flow stress (MPa),  $T$  is the absolute deformation temperature (K),  $R$  is the gas constant ( $\text{J mol}^{-1} \text{K}^{-1}$ ),  $A$  and  $\alpha$  are the material constant,  $n$  is the work hardening constant, and  $Q$  is the apparent activation energy of deformation (kJ/mol).

From Eq 1, it can be inferred:

$$n = \frac{\partial \ln[\sinh(\alpha\sigma)]}{\partial \ln \dot{\epsilon}} \quad (\text{Eq 2})$$

$$Q = Rn \frac{\partial \ln[\sinh(\alpha\sigma)]}{\partial (1/T)} \quad (\text{Eq 3})$$

Assume  $b = \frac{\partial \ln[\sinh(\alpha\sigma)]}{\partial (1/T)}$ , and the activation energy  $Q$  can be defined as:

$$Q = Rnb \quad (\text{Eq 4})$$

The plot of  $\ln \dot{\epsilon}$  versus  $\ln[\sinh(\alpha\sigma_p)]$  and  $\ln[\sinh(\alpha\sigma_p)]$  versus  $1/T$  can be known in Fig. 3, the slopes of which are  $n$  and  $b$ . Respectively, a good linear relationship between  $\ln \dot{\epsilon}$  and  $\ln[\sinh(\alpha\sigma_p)]$  can be found, indicating that the hyperbolic sine Arrhenius constitutive model is suitable for describing the true stress–strain relationship. The average slopes of two graphs can be obtained, and the values of  $n$  and  $b$  are 2.91 and 14.36. The

apparent activation energy of TiAl alloy is determined to be  $347.74 \text{ kJ mol}^{-1}$ .

### 3.2 Fracture Type and Evaluation of Critical Damage Value

In order to find out a suitable fracture criterion for TiAl alloy, it is necessary to understand fracture types and fracture mechanism. There are generally two types that were observed. As shown in Fig. 4, sample appears  $45^\circ$  shear cracking at low temperature (1223 K) and high strain rate ( $1 \text{ s}^{-1}$ ), which is attributed to the inhomogeneity of shear stresses, whereas at higher temperature ( $> 1223 \text{ K}$ ) and lower strain rate ( $< 0.1 \text{ s}^{-1}$ ), the specimen displays the longitudinal cracking and small cracks can be observed in Fig. 4(b), which is the effect of tensile stress caused by deformation of cylindrical sample under thermal compression tests (Ref 29). This demonstrates that the fracture mechanism of Ti-47Al-2Nb-2Cr alloy has a close connection with the hot deformation condition.

Further SEM and STM observations of surface cracking are shown in Fig. 5. At  $1223 \text{ K}/1 \text{ s}^{-1}/60\%$ , many irregular microvoids and a few big equiaxial dimples emerge in addition to plane crystal boundaries, which are created by the plastic deformation after nucleation, growth and aggregation. As temperature increases and strain rate decreases, the crystal plane becomes much smoother and microvoids are round in shape (Fig. 5c). Besides, a number of equiaxial dimples appear in Fig. 5(d), which show better plasticity of the material. It seems that working parameters plays an important role in the fracture and deformation non-uniformity.

The fracture mode can be obtained according to the BSE images of TiAl alloy. As shown in Fig. 6(a), microcrack appears in the boundaries of planer crystal boundaries, which

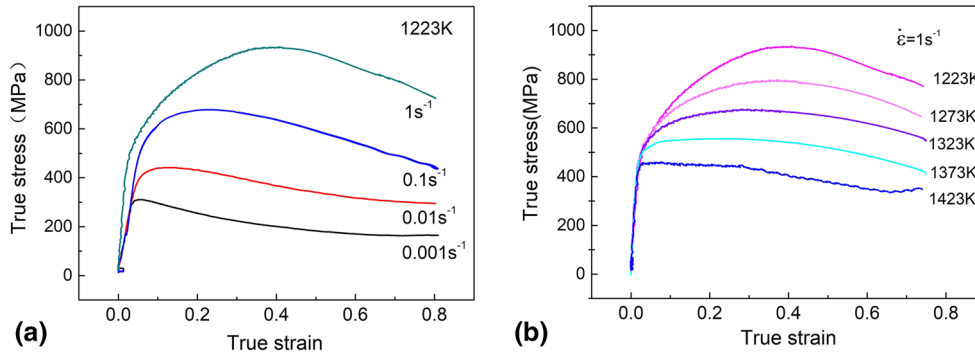


**Fig. 2** True stress–true strain curves at different strain rates and temperature: (a) 1223 K (b)  $1 \text{ s}^{-1}$

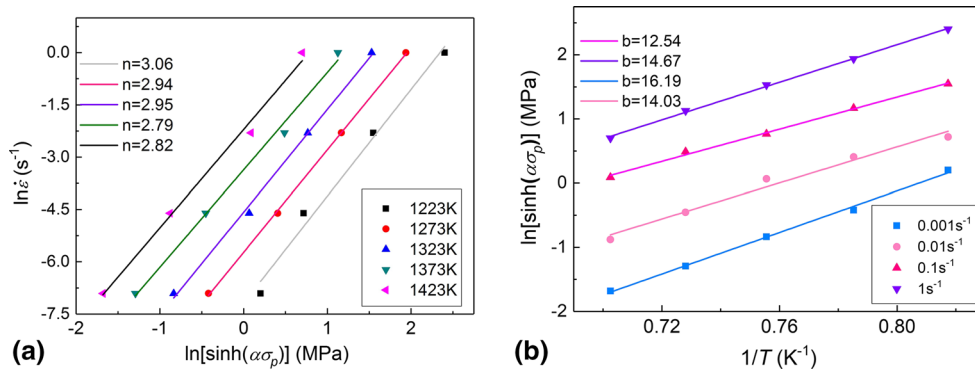


**Fig. 3** Relationships between stress and strain rates and temperature

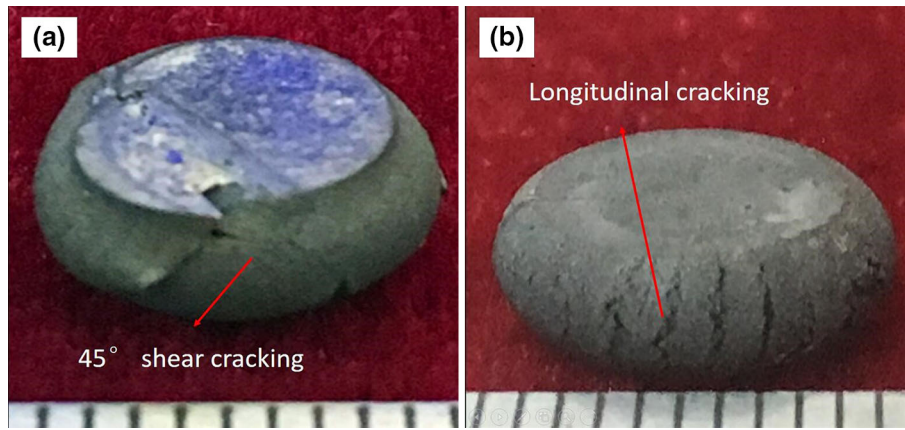


**Fig. 4** Macrophotography of hot deformed specimens: (a) 1223 K/1 s<sup>-1</sup>/60%, (b) 1323 K/0.1 s<sup>-1</sup>/60%

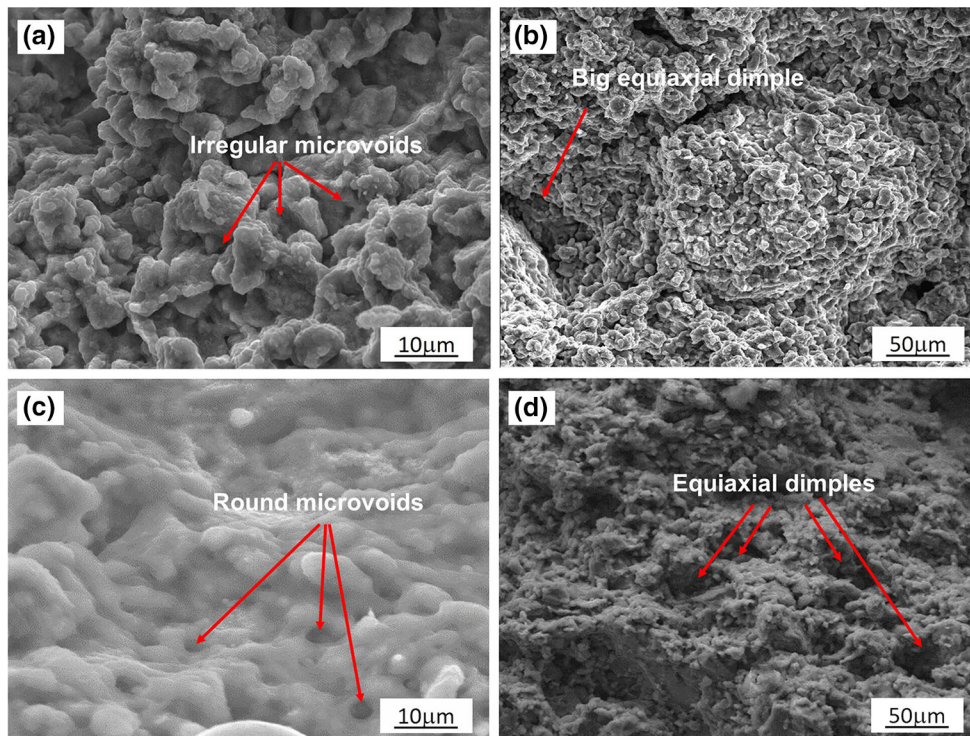


**Fig. 5** Fractographs at various hot deformation conditions: (a, b) 1223 K/1 s<sup>-1</sup>/60%, (c, d) 1323 K/0.1 s<sup>-1</sup>/60%

illustrates intergranular fracture is the major way of fracture mode. In the condition of temperature growing and strain rate falling, cracks appear through some crystalline grains, indicating the fracture model is mixed with transgranular and intergranular fracture (Fig. 6b). Bieler (Ref 31) also observed mixed transgranular and intergranular cracks in the bi-phase TiAl alloy. This fracture mode is consisted with the conclusion obtained by other researchers (Ref 32).

The increasing temperature and decreasing strain rate not only turn the intergranular binding force becomes weak, but also increase the content of  $\alpha_2$ -Ti<sub>3</sub>Al phase as shown in Fig. 7. The small increase in second phase contributes to the refining of  $\gamma$ -TiAl phase through absorbing impurity element of alloy and also reduces the content of Al in  $\gamma$ -TiAl phase, which is considered to be beneficial to the plasticity improvement.

Besides, the content of the  $\alpha_2$ -Ti<sub>3</sub>Al phase is considered to be related to the size of dimple formation.

Chen and Kim (Ref 30) considered that the fracture mechanism of TiAl alloy is the function of temperature, strain rate and other parameters. Among them, critical fracture strain is thought to be a basic experimental threshold data which has significant effect on the accuracy of the fracture model. Therefore, how to obtain the accurate critical fracture strain has been an imperative problem that many researchers are still studying. Although several new methods such as infrared thermography (Ref 33) and high-speed photography (Ref 34) have been applied, classical dichotomy research remains as the most believable and reasonable one among other approaches without highly sophisticated testing equipment. Consequently, bisection method is applied in this work to obtain the threshold

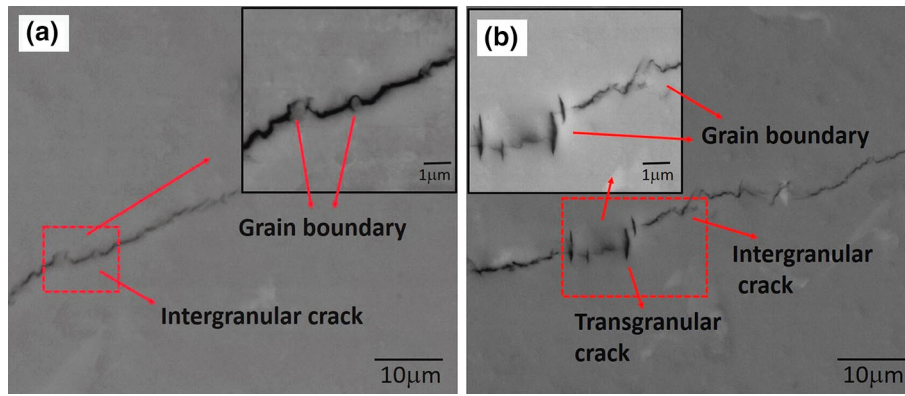


**Fig. 6** The microcrack at various hot deformation conditions: (a) 1223 K/1 s<sup>-1</sup>/60%, (b) 1323 K/0.1 s<sup>-1</sup>/60%

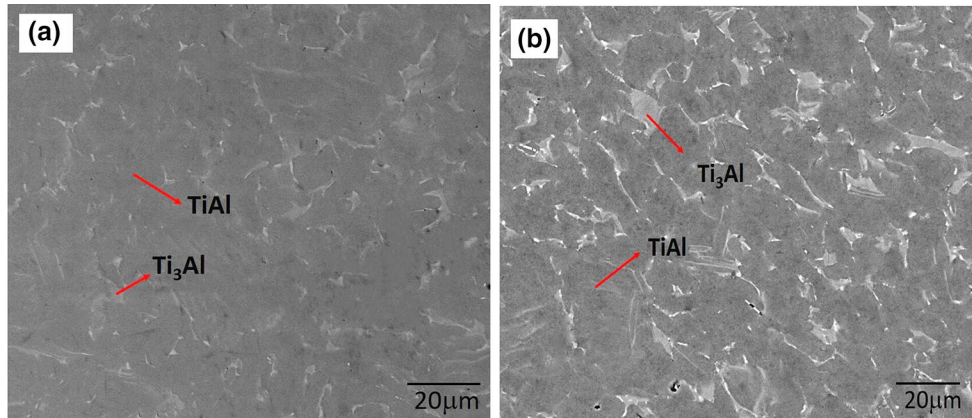


**Fig. 7** Deformed microstructure at various processing conditions: (a) 1223 K/1 s<sup>-1</sup>/60%, (b) 1323 K/0.1 s<sup>-1</sup>/60%

fracture strain. It is generally known that critical fracture strain in certain condition cannot be determined before hot compressing experiment, in another word, when the fracture of sample would occur during tests cannot be predicted precisely in advance. However, by several experimental trials, the strain scope between fracture and fracture free of samples can be obtained. Afterward, the scope can be narrowed by dichotomy to a required accuracy to determine the threshold damage strain. For instance, in the hot compression test, assuming that fracture doesn't occur in 40% reduction of specimen, while it does in 60%, the diminution scope can be made sure between 40 and 60%. According to the theory of dichotomy, 50% reduction compressing experiment should be conducted. If the sample begins to crack at the 50% of deformation rate, 45% test is going to be carried out. With the experiment going on, the requested accuracy of critical damage strain can be achieved.

In terms of the above approach, the critical fracture strain at each working condition can be acquired. Figure 8 shows impacts of temperature as well as the strain rate on the threshold fracture strain value. It can be known that 3-D deformation space was divided into two areas by critical damage surface, which upper and lower were fracture zone and safe zone. As expected, threshold damage strain grows with increasing temperature and decreasing strain rate in most compressing tests. On the other hand, in the range of high deformation temperature ( $\geq 1373$  K) and low strain rate ( $= 0.001$  s<sup>-1</sup>), threshold damage strain decreased with the elevated temperature growing, showing a reduced processabil-

ity at higher temperature range. The weak processability could be connected with the crude grains. Therefore, the most appropriate deformation temperature is less than 1373 K. In addition, there is no doubt that low strain rate is beneficial for large plastic deformation with the low efficiency.

#### 4. Establishing the Thermal Deformation Failure Model

Five representative theoretical fracture criteria are reviewed in Table 1, and it can be known that the establishment of above-mentioned criteria is based on physical experiments as well as microstructure analysis of cold deformation. Nevertheless, this paper investigates the fracture behavior under metal-forming processes with heating temperature. A significant characteristic that tells the difference between hot deformation behavior and cold one is two processing factors ( $T$  and  $\dot{\epsilon}$ ), which have great effects on thermally activated processes and dynamic softening. Particularly, variation of working parameters plays an important role on the threshold cracking. In addition, one common feature between hot and cold deformation is that the stress and strain histories strongly affect the initiation of ductile fracture, which is the reason that most failure criteria exhibit the expression that ductile fracture occurs when the damage parameters provided with integral of stress as well as strain, comes to a threshold. Therefore, to achieve the purpose of

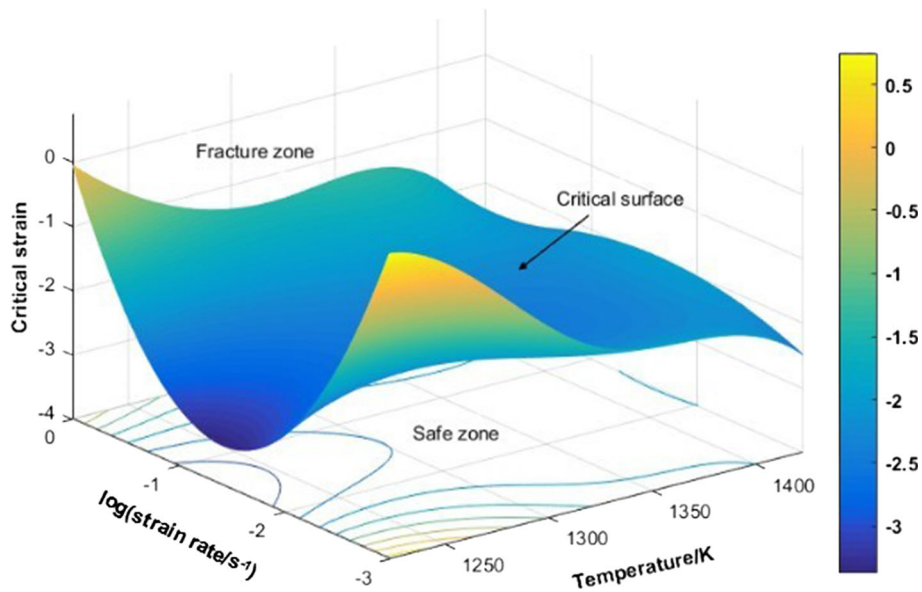


Fig. 8 The relationship between critical strain and strain rates and temperature

Table 1 The typical ductile fracture criteria

Criteria	Physical formula	Background	Ref
Freudenthal	$\int_0^{\epsilon_f} \bar{\sigma} d\bar{\epsilon} = C$	Plastic work	13
Cockcroft and Latham	$\int_0^{\epsilon_f} \sigma_1 d\bar{\epsilon} = C$	Empirical model	14
Brozzo	$\int_0^{\epsilon_f} \frac{2\sigma_1}{3(\sigma_1 - \sigma_H)} d\bar{\epsilon} = C$	Cumulative plastic energy models	15
Oh and Kobayashi	$\int_0^{\epsilon_f} \frac{\sigma_1}{\bar{\sigma}} d\bar{\epsilon} = C$		16
Oyane	$\int_0^{\epsilon_f} (1 + \frac{\sigma_H}{A\bar{\sigma}}) d\bar{\epsilon} = C$	Microdamage models	19

simplicity, the new modeling procedure is divided into two steps as follows: first, a suitable criterion is determined among the universal cold deformation criteria; then, a failure criterion applied to thermal deformation is established by bringing in  $T$  and  $\dot{\epsilon}$ .

The selected fracture criteria from publication are shown in Table 1, which are performed by means of damage energy accumulation through stress and strain. The variables like equivalent stress ( $\bar{\sigma}$ ), hydrostatic stress ( $\sigma_H$ ), as well as maximum principal stress ( $\sigma_1$ ) have close associated with fracture initiation. After establishing a library of Ti-47Al-2Nb-2Cr alloy and selecting criteria in the finite element simulation platform, simulation experiments are conducted to calculate variation of samples during thermal upsetting tests at 1223 K/0.1 s<sup>-1</sup>. The curves of Fig. 9 present the change trend of damage values with the distance from the center of deformed samples. As illustrated in Fig. 9, the damage parameter calculated by Freudenthal, Cockcroft and Latham, Brozzo as well as Oyane criteria comes to its maximum value at the equator of cylindrical sample. According to Oh and Kobayashi criterion, the maximum fracture value appears on the top surface and free surface of sample. The maximum damage by Oh and Kobayashi criterion appeared suddenly in the random zone of specimen without gradually change like the other criteria. Heading deformation processes are usually depicted by com-

pressive stress, which equivalent stress and maximum principal stress increased with the deformation processes, nevertheless, the various ratio of maximum principal stress and equivalent stress cannot be determined in particular, owing to the ratio of maximum principal stress and equivalent stress is negative value. In addition, Oh and Kobayashi criterion considers the effect ratio between maximum principal pressure and equivalent stress. Consequently, damage value calculated by Oh and Kobayashi criterion is conflicting. Similar features from the rest four criteria reveal the curves of damage value rise with the increasing distance from the center of cylindrical sample. In terms of the statement of fracture criteria, damage value is supposed to reach its maximum at the damage position; therefore, the maximum is referred to as critical damage value. By observing the crack specimens, it can be found that the damage position is at the equatorial plane on the bulge; hence, Oh and Kobayashi criterion is considered improper for modeling thermal deformation failure criterion of Ti-47Al-2Nb-2Cr alloy.

For the purpose of further selecting a most suitable criterion in the remaining parts (Freudenthal, Cockcroft and Latham, Brozzo, Oyane), additional simulation experiments under different deformation circumstance (1223-1423 K, 0.001-1 s<sup>-1</sup>) were performed and the critical fracture values acquired from rest of criteria were extracted and analyzed. The

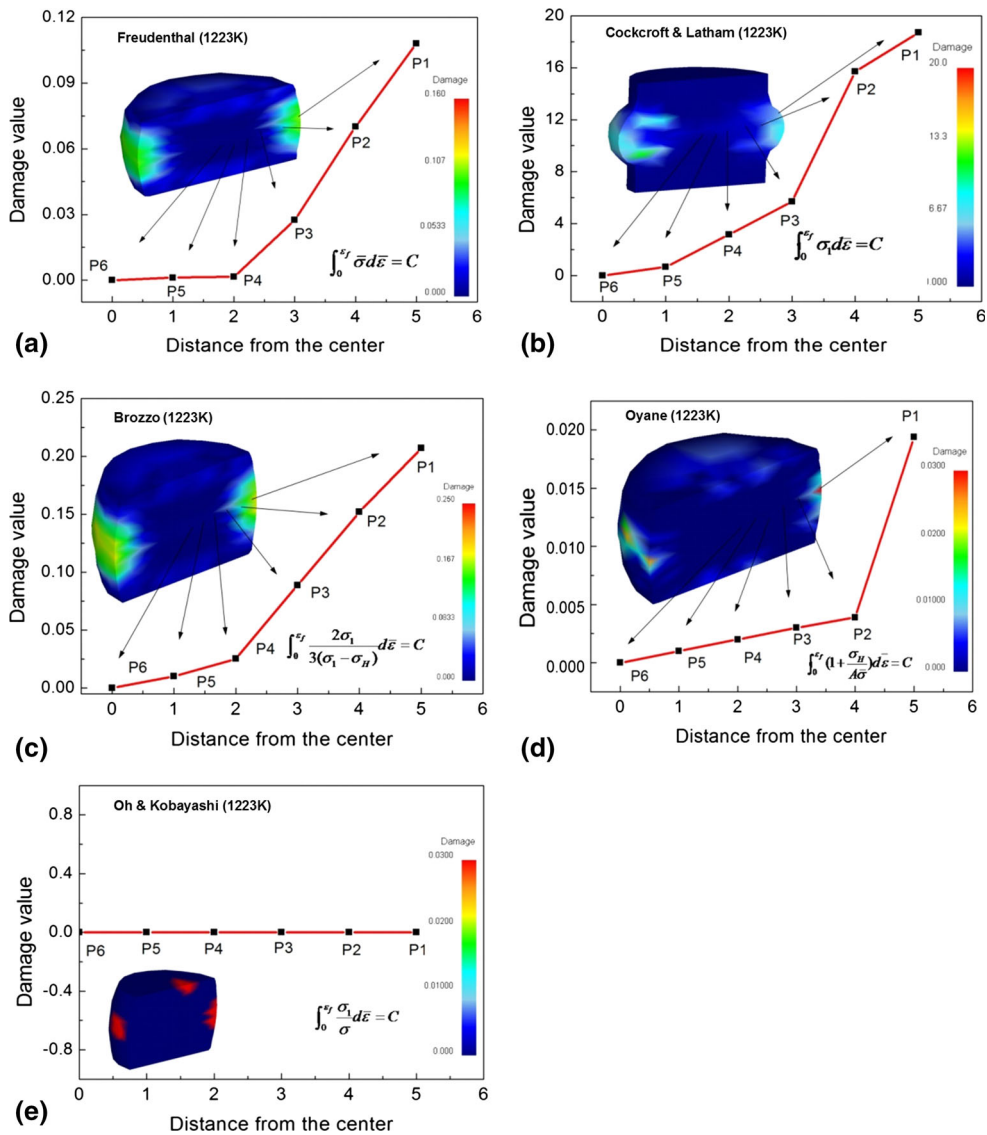


**Fig. 9** Damage value distributions from axis to free surface under hot deformation based on different fracture criteria: (a) Freudenthal, (b) Cockcroft and Latham, (c) Brozzo, (d) Oyane, (e) Oh and Kobayashi

relationship between critical fracture values and working parameters under four criteria can be known in Fig. 10. In general, it can be well known that threshold damage values increase continuously with growing of working temperature as well as reducing of strain rate. Because the metal shows a good plastic deformation ability under the heated and slow processing state, which critical fracture results are considered to come to a high level until damage occurs. Obviously, Cockcroft and Latham and Oyane criterion do not conform to the criterion, and curves about Freudenthal criterion at high temperature ( $> 1373$  K) do not go higher with the increase of temperature illustrating that it is not in line with the criterion, too. Therefore, compared with the other three criteria, Brozzo criterion is the most appropriate choice for modeling the thermal working damage criterion of Ti-47Al-2Nb-2C alloy.

Since the critical fracture values have high correlation with the deformation parameters (strain rate and temperature), the new established damage model based on Brozzo criterion can be expressed in Eq 5:

$$\int_0^{\bar{\epsilon}_f} \frac{2\sigma_1}{3(\sigma_1 - \sigma_H)} d\bar{\epsilon} = C_f = f(T, \dot{\epsilon}) \quad (\text{Eq 5})$$

In Eq 5,  $\sigma_1$  is maximum principal stress (MPa);  $\sigma_H$  is hydrostatic stress (MPa);  $C_f$  is fracture value of Brozzo criterion;  $\bar{\epsilon}$  is equivalent strain when initial fracture occurs;  $T$  is Kelvin temperature (K), and  $\dot{\epsilon}$  is strain rate ( $s^{-1}$ ). Zener-Hollomon parameter is usually introduced to replace the two variables ( $T$  and  $\dot{\epsilon}$ ), which is expressed in Eq 6.

$$Z = \dot{\epsilon} \exp\left(\frac{Q}{RT}\right) \quad (\text{Eq 6})$$

where  $\dot{\epsilon}$  is strain rate ( $s^{-1}$ ),  $T$  is absolute temperature (K),  $Q$  is activation energy ( $\text{KJ mol}^{-1}$ ), and  $R$  is the gas constant ( $\text{KJ mol}^{-1} \text{K}^{-1}$ ). As  $Z$  parameter presents a corporate influence of temperature and strain rate, using  $Z$  parameter to express those variables ( $T, \dot{\epsilon}$ ) is applicable.

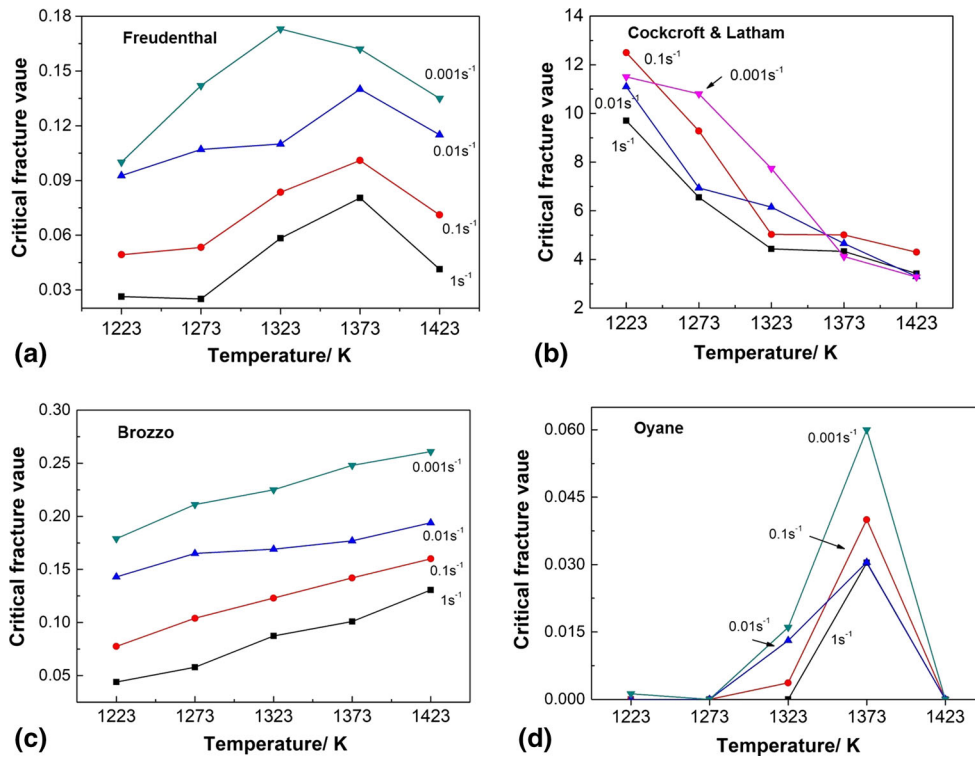


**Fig. 10** Critical cracking distribution for different cracking criteria at different temperature and strain rates: (a) Freudenthal criterion, (b) Cockcroft and Latham criterion, (c) Brozzo criterion, (d) Oyane criterion

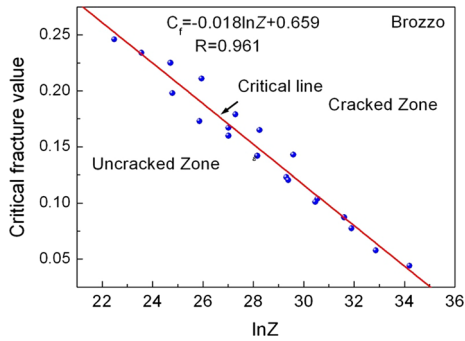


**Fig. 11** Relationship of Brozzo criterion between critical fracture value ( $C_f$ ) and  $\ln Z$

Figure 11 illustrates that the critical fracture value ( $C_f$ ) of the Brozzo criterion has a great linear relationship with the  $\ln Z$ . The correlation coefficient ( $R$ ) of the regression curve is 0.961, which demonstrates the validness of the established relationship. If the fracture value ( $C$ ) calculated by the formula ( $C > C_f$ ) is in the zone above the critical line, the fracture of metal will occur at the given condition in the practical experiment. Meanwhile, the correlation of critical fracture value and  $\ln Z$  indicates that hot working parameters ( $T, \dot{\epsilon}$ ) have great influence on metal fracture during deformation processes in addition to stress and strain. Therefore, the damage criterion of hot forming based on Brozzo criterion was established as follows in Eq 7:

$$C_f = \int_0^{\bar{\epsilon}_f} \frac{2\sigma_1}{3(\sigma_1 - \sigma_H)} d\bar{\epsilon} = -0.018 \ln Z + 0.659 \quad (\text{Eq 7})$$

$$= -0.018 \left( \ln \dot{\epsilon} + \frac{Q}{RT} \right) + 0.659$$

The fracture model based on the Brozzo criterion of Ti-47Al-2Nb-2Cr alloy under hot deformation conditions in Eq 7 can be also expressed in another way like Eq 8.

$$C_i = \frac{1}{C_f} \sum_{\bar{\epsilon}_i=1}^n \frac{2\sigma_1}{3(\sigma_1 - \sigma_H)} d\bar{\epsilon} \quad (\text{Eq 8})$$

where  $C_i$  is the integral value,  $C_f$  is the critical fracture value, which is determined by hot deformation conditions. When  $C_i < 1$ , it is considered that no fracture occurred, and when  $C_i > 1$ , the sample is thought to crack.

The new fracture model was put into the finite element method based (FEM) software DEFORM-3D by FORTRAN language for secondary development. The flow diagram of FE program covering subprogram of new damage model can be known in Fig. 12. When the deformation temperature, strain rate and other parameters were set, the more accurate initial damage position as well as critical strain value could be calculated by operations of FE programs.

In order to test and verify the new established criterion, the contrast experiments between physical experimental and predictive results about initial cracking position and threshold damage strain of alloy at 1293 K/0.5 s<sup>-1</sup>, 1293 K/0.1 s<sup>-1</sup>, 1243 K/0.5 s<sup>-1</sup> and 1243 K/0.1 s<sup>-1</sup> have been conducted. From Fig. 13, the predicted maximum damage at 1293 K/



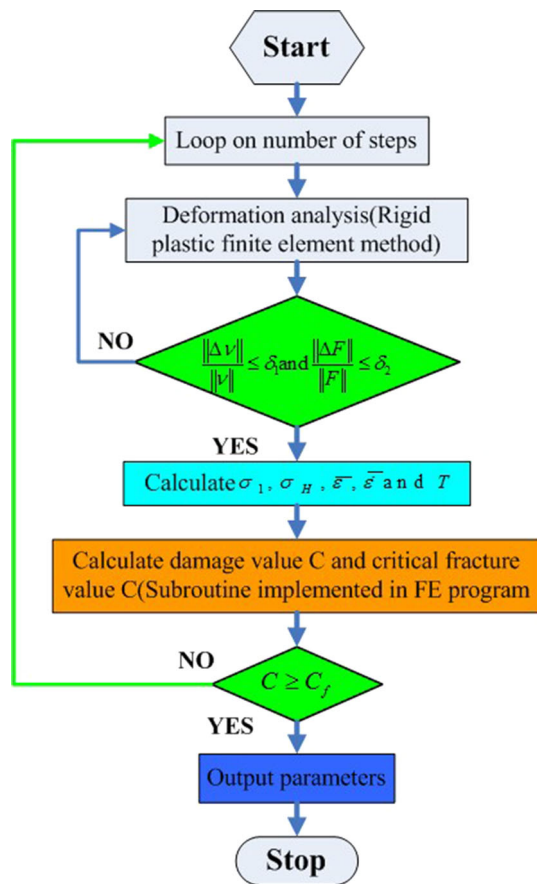


**Fig. 12** Flow diagram of FE procedure covering subprogram of hot deformation damage model

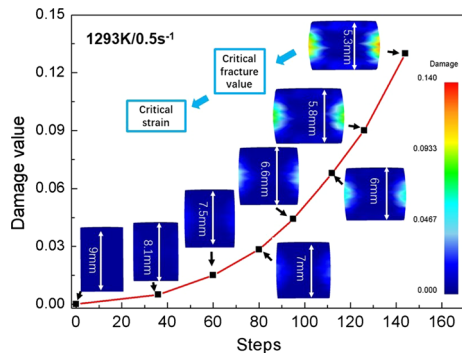


**Fig. 13** Prediction of fracture by means of FEM

**Table 2** Experimental and simulated critical strain after compression at different conditions

Temperature, K	Strain rate, s <sup>-1</sup>	Experimental critical strain	Simulated critical strain	Relative deviation, %
1293	0.5	0.375	0.400	6.7
1293	0.1	0.475	0.455	4.2
1243	0.5	0.350	0.320	9.4
1243	0.1	0.463	0.480	3.7

0.5 s<sup>-1</sup> is located in the equatorial plane on the bulge of sample, which is in great coherence with experimental evidences. In terms of the maximum damage value obtained from the new model, the critical strain calculated by the FE subroutine is 0.4, which is close to the experimental value (0.375), demonstrating the correctness of the FE subroutine running in the main program loop. Simulation results in other deformation conditions (Table 2) match experimental values well and the relative error do not reach 9.4%. Consequently, the fracture prediction model adopting a combined method of ductile fracture criteria theory and FEM technique is reasonable and has practical reference value.

## 5. Conclusions

Thermal deformation performance of Ti-47Al-2Nb-2Cr alloy was researched according to upsetting experiments within 1223-1423 K as well as 0.001-1 s<sup>-1</sup>. Combined with processing experiments, theoretical fracture criteria and FE simulation, a damage prediction criterion which describes the relationship of ductile fracture and hot processing parameters has been established. The main conclusions are as follows:

- 45° shear crack appears at the temperature of 1223 K and strain rate of 1 s<sup>-1</sup>, which intergranular fracture is responsible for macrofracture. Longitudinal cracking and small cracks are found at higher temperature (> 1223 K) and lower strain rate (< 0.1 s<sup>-1</sup>), which the failure model considers both transgranular and intergranular fracture.
- The peak stress of TiAl alloy can be depicted by hyperbolic sine-type equation, and then the thermal activation energy is calculated to be approximately 347.74 kJ mol<sup>-1</sup>. Critical damage strain grows with increasing temperature as well as decreasing strain rate. The most appropriate deformation temperature is less than 1373 K.
- The established relationship about critical fracture value and Zener-Hollomon parameter is exponential decrease. The fracture model for Ti-47Al-2Nb-2Cr alloy under hot deformation conditions was established as a function of stress, strain, temperature and strain rate. This model can accurately predict the cracking position and critical strain of the alloy within a certain range.

## Acknowledgments

This work was sponsored by National Natural Science Foundation of China (Grant No.51405110), the Fundamental Research Funds for the Central Universities (Grant No. HIT. NSRIF. 2014006), the Specialized Research Fund for the Doctoral Program of Higher Education (Grant No.20132302120002) and the China Postdoctoral Science Foundation (Grant No.2014M551234).

## Author Contributions

Zhuohan Cao and Yu Sun conceived and designed the project. Zhuohan Cao and Zhipeng Wan performed the thermal compression experiments. Zhuohan Cao carried out the SEM and BSE experiments, simulated and analyzed the data by using Deform 3D software. Zhuohan Cao, Yu Sun, Zhipeng Wan, Lianxi Hu contributed to the interpretation, discussion of the data and the writing of the paper.

## Conflict of Interest

The authors declare no conflict of interest

## References

1. F. Appel and R. Wagner, Microstructure and Deformation of Two-Phase  $\gamma$ -Titanium Aluminides, *Mater. Sci. Eng., R*, 1998, **22**, p 187–268
2. H. Clemens and S. Mayer, Design, Processing, Microstructure, Properties, and Applications of Advanced Intermetallic TiAl Alloys, *Adv. Eng. Mater.*, 2013, **15**, p 191–215
3. L. Chen, J. Li, X. Xue, B. Tang, K. Kou, and E. Bouzy, General Features of High Temperature Deformation Kinetics for  $\gamma$ -TiAl-Based Alloys with DP/NG Microstructures: Part I. A Survey of Mechanical Data and Development of Unified Rate-Equations, *Mater. Sci. Eng., A*, 2016, **648**, p 389–401
4. H. Saage, A.J. Huang, D. Hu, M.H. Loretto, and X. Wu, Microstructures and Tensile Properties of Massively Transformed and Aged Ti46Al8Nb and Ti46Al8Ta, *Intermetallics*, 2009, **17**, p 32–38
5. Y.M. Kim, and T. Carneiro, Role of Niobium in the Process of Gamma Alloy Development. Niobium: High Temperature Applications, Proceedings, in *International Symposium on Niobium for High Temperature Applications, Araxa, Brazil*, 01–03, December, 2003, pp. 125–137
6. D.M. Dimiduk, Gamma Titanium Aluminide Alloys—an Assessment Within the Competition of Aerospace Structural Materials, *Mater. Sci. Eng., A*, 1999, **263**, p 281–288
7. H. Jiang, S. Zeng, A. Zhao, X. Ding, and P. Dong, Hot Deformation Behavior of  $\beta$  Phase Containing  $\gamma$ -TiAl Alloy, *Mater. Sci. Eng., A*, 2016, **661**, p 160–167
8. S.V.S. Narayana Muryt, B. Nageswara Rao, and B.P. Kashyap, Identification of Flow Instabilities in the Processing Maps of AISI, 304 Stainless Steel, *J. Mater. Process. Technol.*, 2005, **166**, p 268–278
9. A. Venugopal Rao, N. Ramakrishnan, and R. Krishna Kumar, A Comparative Evaluation of the Theoretical Failure Criteria for Workability in Cold Forging, *J. Mater. Process. Technol.*, 2003, **142**, p 29–42
10. B.P.P.A. Gouveia, J.M.C. Rodrigues, and P.A.F. Martins, Ductile Fracture in Metalworking: Experimental and Theoretical Research, *J. Mater. Process. Technol.*, 2000, **101**, p 52–63
11. H.A. Kuhn, P.W. Lee, and T. Erturk, A Fracture Criterion for Cold Forming, *J. Eng. Mater. Technol.*, 1973, **95**, p 213–218
12. V. Vujovic and A.H. Shabaik, A New Workability Criterion for Ductile Metals, *J. Eng. Mater. Technol.*, 1986, **3**, p 245–249
13. A.M. Freudenthal, *The Inelastic Behavior of Engineering Materials and Structures*, Wiley, New York, 1950, p 1–70
14. M.G. Cockcroft, and D.J. Latham, A simple Criterion of Fracture for Ductile Metals. UK National Engineering Laboratory Report, 1966, p. 240
15. P. Brozzo, B. Deluca, and R. Rendina, A new Method for the Prediction of Formability Limits in Metal Sheet, in *Proceedings of the 7th Biennial Conference on IDDR*, 1972.
16. S.H. Oh, C.C. Chen, and S. Kobayashi, Ductile Fracture in Axisymmetric Extrusion and Drawing-Part 2: Workability in Extrusion and Drawing, *J. Manuf. Sci. Eng.*, 1979, **101**, p 33–34
17. F.A. McClintock, Challenges in Fracture Mechanics, *Dev. Mech.*, 1969, **5**, p 905–919
18. J.R. Rice and D.M. Tracey, On the Ductile Enlargement of Voids in Triaxial Stress Fields, *J. Mech. Phys. Solids*, 1969, **17**, p 201–217
19. Z. Oyane, Criteria of Ductile Fracture Strain, *Bull. JSME*, 1972, **15**, p 1507–1513
20. M. Ayada, T. Higashino, and K. Mori, Central Bursting in Extrusion of Inhomogeneous Materials, *Adv. Technol. Plast.*, 1987, **1**, p 553–558
21. S. Kobayashi, and C.H. Lee, Deformation Mechanics and Workability in Upsetting Solid Circular Cylinders, in *Proceeding of the North American Metalworking Research Conference*, 1973, Vol 1
22. A.S. Wifi, N. El-Abbasi, and A. Abdel-Hamid, A Study of Workability Criteria in Bulk Forming Processes, *Stud. Appl. Mech.*, 1995, **43**, p 333–357
23. A.S. Wifi, A. Abdel-Hamid, and N. El-Abbasi, Computer-Aided Evaluation of Workability in Bulk Forming Processes, *J. Mater. Process. Technol.*, 1998, **77**, p 285–293
24. H. Li, M. Fu, J. Lu, and H. Yang, Ductile Fracture: Experiments and Computations, *Int. J. Plast.*, 2011, **27**, p 147–180
25. W. Zhang, Y. Liu, H.Z. Li, Z. Li, H. Wang, and B. Liu, Constitutive Modeling and Processing Map for Elevated Temperature Flow Behaviors of a Powder Metallurgy Titanium Aluminide Alloy, *J. Mater. Process. Tech. Technol.*, 2009, **209**, p 5363–5370
26. P.W. Wilson, *Recent Developments in the Study of Recrystallization*, Rijeka, In Tech, 2013, p 61–66
27. S.M. Mohseni, A.B. Phillion, and D.M. Maijer, Modelling the Constitutive Behaviour of Aluminium Alloy B206 in the As-Cast and Artificially Aged States, *Mater. Sci. Eng., A*, 2016, **649**, p 382–389
28. F. Jiang, H. Zhang, J. Su, and Y. Sun, Constitutive Characteristics and Microstructure Evolution of 7150 Aluminium Alloy During Isothermal and Non-isothermal Multistage Hot Compression, *Mater. Sci. Eng., A*, 2015, **636**, p 459–469
29. Y. Zhu, W. Zeng, F. Zhang, Y. Zhao, X. Zhang, and K. Wang, A New Methodology for Prediction of Fracture Initiation in Hot Compression of Ti40 Titanium Alloy, *Mater. Sci. Eng., A*, 2012, **553**, p 112–118
30. K.S. Chan and Y.W. Kim, Effects of Lamellae Spacing and Colony Size on the Fracture Resistance of a Fully-Lamellar TiAl Alloy, *Acta Metall. Mater.*, 1995, **43**, p 439–451
31. T.R. Bieler, A. Fallahi, B.C. Ng, D. Kumar, M.A. Crimp, B.A. Simkin, A. Zamiri, F. Pourboghrat, and D.E. Mason, Fracture Initiation/Propagation Parameters for Duplex TiAl Grain Boundaries Based on Twinning, Slip, Crystal Orientation, and Boundary Misorientation, *Intermetallics*, 2005, **13**(9), p 979–984
32. X. Zan, H.Y. He, Y. Wang, and Y.M. Xia, Dynamic Behavior and Fracture Mode of TiAl Intermetallics with Different Microstructures at Elevated Temperatures, *Trans. Nonferrous Met. Soc. China*, 2011, **21**(1), p 45–51
33. S. Punnose, A. Mukhopadhyay, R. Sarkar, Z. Alam, D. Das, and V. Kumar, Determination of Critical Strain for Rapid Crack Growth During Tensile Deformation in Aluminide Coated Near- $\alpha$  Titanium Alloy Using Infrared Thermography, *Mater. Sci. Eng., A*, 2013, **576**, p 217–221
34. X. Zhang, W. Zeng, Y. Shu, Y. Zhou, Y. Zhao, H. Wu, and H. Yu, Fracture Predicting of Ti40 Burn Resistant Titanium Alloy in Hot Forming, *Rare Met. Mater. Eng.*, 2006, **35**, p 1900–1903